J Mater Sci: Mater Electron (2017) 28:8630–8642
DOI 10.1007/s10854-017-6587-1

Magnetocoupling and domain structure of $BiFeO_3$/ $LaFeO_3$ heterostructures deposited on $LaSrCoO_3$/Pt/TiO_2/SiO_2/Si (100) substrates by the soft chemical method

R. C. Deus[1] · L. F. Gonçalves[1] · C. C. Cavalcanti[1] · L. S. R. Rocha[1] · E. Longo[2] · A. Z. Simões[1]

Received: 16 December 2016 / Accepted: 14 February 2017 / Published online: 21 February 2017

Abstract $BiFeO_3$ (BFO) and $LaFeO_3$ (LFO) heterostructures were obtained at room temperature on Pt/TiO_2/SiO_2/Si (100) substrates by chemical solution deposition at a temperature of 500 °C for 2 h. For comparison, the films were also deposited on $La_{0.5}Sr_{0.5}CoO_3$ coated Pt/TiO_2/SiO_2/Si (100) substrates. The magnetoelectric coefficient measurement was performed to show magnetoelectric coupling behavior of such heterostructures. $La_{0.5}Sr_{0.5}CoO_3$ (LSCO) bottom electrode strongly promotes the formation of high intensity (104) texture of *BFO-LFO* heterostructures resulting in huge crystal size. The dielectric constants of the films increased from 307 to 400 at 1 MHz with the bottom electrode while the leakage current behavior at room temperature of the films decreased from 10 to 10–10^{-7} A/cm^2 at a voltage of 5 V. Improvement of the *P–E* hysteresis loop was observed for the heterostructure due the decrease of leakage current caused by the LFO sublayer. Room temperature magnetic coercive field measurements indicate that the magnetic behavior is influenced by the nature of bottom electrode.

✉ A. Z. Simões
alezipo@yahoo.com

[1] Faculdade de Engenharia de Guaratinguetá, Universidade Estadual Paulista (UNESP), Av. Dr. Ariberto Pereira da Cunha, 333, Bairro Portal das Colinas, CEP 12516-410 Guaratinguetá, SP, Brazil

[2] Instituto de Química - Laboratório Interdisciplinar em Cerâmica (LIEC), Universidade Estadual Paulista (UNESP), Rua Professor Francisco Degni s/n, Araraquara, SP 14800-90, Brazil

1 Introduction

Revival in multiferroic materials brings ever-increasing enthusiasm in the research of this field [1]. Several promising materials such as $YMnO_3$ [2] $LuFe_2O_4$ [3] $BiFeO_3$ (BFO) [4] and BiMnO3 [5], are currently under intensive studies. Among them, BFO receives most of the interest due to its room temperature ferroelectric and magnetic orders [6, 7]. In the traditional chemical method for preparing BFO based films, generally Pt/Ti/SiO_2/Si has been used as substrate. However, the poor ferroelectric-electrode interface prevents the full expression of the outstanding ferroelectric behavior of BFO thin films [8]. Ferroelectric ferromagnets (or ferrimagnets) are very scarce and the quest for a material with both large finite polarization and magnetization at room temperature is still in progress. To reach this goal, it is neccessary to obtain materials with magnetoelectric coupling. Among all known multiferroics, the only compound that satisfies these criteria is $BiFeO_3$ (BFO). First synthesized in the late 1950s by Kiselev et al. [7, 9], BFO was shown to be a G-type antiferromagnet with a Néel temperature of 630 K. Later, Sosnowska et al. showed that the magnetic order of bulk BFO is not strictly collinear and that a cycloidal modulation with a period of 62 nm is present [10]. Although some methods have been used to decrease the current density leakage of BFO thin films, their electrical behavior is still not ideal [11–14]. Among these promising methods, the bilayered structure consisting of BFO and other ferroelectrics may be a more promising method for decreasing the leakage current density and improving the electrical properties of BFO, because of the bilayered structure. The bilayered thin films consisting of BFO and one other ferroelectric layer have been reported [12–14], such as $Bi_{1/2}Na_{1/2}TiO_3$, $Pb(Zr,Ti)O_3$. Some interesting results have been demonstrated by such a bilayered

structure, such as the reduction in current density leakage, the improvement in phase purity, and the enhancement in fatigue behavior, but their polarization value is much lower as compared with the intrinsic polarization of BFO thin films. In the present work, the bilayered thin films consisting of $BiFeO_3$ and $LaFeO_3$ were grown *in situ* on Pt/TiO_2/SiO_2/Si (1 0 0) and $La_{0.5}Sr_{0.5}CoO_3$ coated Pt/TiO_2/SiO_2/Si (1 0 0) substrates by the chemical solution deposition method. Lanthanum orthoferrite $LaFeO_3$ (LFO) is a perovskite oxide with semi-conducting behavior [15], and has been extensively studied with reference to several potential applications, such as in gas sensors and as an electrode material in solid-state fuel cells (SOFC) [16]. This oxide crystallizes in an orthorhombically distorted perovskite structure with anti-ferromagnetic characteristics [17]. The particular characteristics of anti-ferromagnetism and an extremely high ordering temperature (T_N) are very promising for the use of the material in the storage industry, in spin valves, in exchange bias applications and in heterostructures of magnetic/magnetic and magnetic/electric films [18–21]. The magnetoelectric (ME) coefficient $\alpha ME = dE/dH = dV/(tdH)$ is the most critical indicator for the magnetoelectric coupling properties in multiferroic materials, where V is the induced magnetoelectric voltage, H is the exciting ac magnetic field, and t is the thickness of the sample used for measuring V across the laminate [21]. Among the various approaches to improve the magnetoeletric coupling in BFO thin films, a combination of antiferromagnetic (AFM) layer consisting of LFO is a promising candidate to improve the coupling between the magnetic and polarization states of the BFO. AFM layers play a key role in such magnetoeletronic device applications, where they serve to pin an adjacent ferromagnetic (*FM*) layer by force of the exchange-bias coupling [22]. The interest in exchange-biased nanostructures has accelerated recently, as a result of advances in fabrication methods and the emergence of novel tools for characterization of magnetic and electrical properties with high spatial resolution. Conductive oxides with perovskite structure are expected to have much better affinity with a ferroelectric oxide which is more advantage for the interfacial properties between the conductive and ferroelectric oxides because of their similar crystal structures. So far, conductive oxides, such as $SrRuO_3$, $La_{0.5}Ca_{0.5}CoO_3$, $LaNiO_3$ (LNO), and $BaPbO_3$, [23–25] have been investigated and employed as electrodes to minimize the fatigue and aging of ferroelectric films, which is of the fundamental importance for the practical applications in multifunctional devices. Among these oxide electrode materials, $LaSrCoO_3$ (LSCO), which is a perovskite related metallic oxide [26], has also attracted much attention in recent years, as a conduction layer for application in ferroelectric memories. Because LSCO has a structure similar to that of perovskite ferroelectrics, textured and epitaxially grown LSCO film is a promising oxide electrode. At present, most epitaxial LSCO films have been prepared by physical processes such as pulsed laser deposition (PLD) [27] and RF magnetron sputtering [28]. LSCO has low resistivity and pseudo-cubic perovskite structure with lattice parameter 0.3835 nm, which is compatible with that of BFO (i.e., 0.396 nm). It is easy to fabricate LSCO on Pt coated Si substrate via a chemical route, and moreover, LSCO is inclined to grow in (111)-preferential orientation; Thus, it is likely to induce the growth of BFO films in (111) orientation. All of these make it a good choice as buffer layer and bottom electrode. In this study we report the growth of effect of La-substituted BFO films deposited on LSCO/Pt/TiO_2/SiO_2/Si (100) Si substrates by using the polymeric precursor method and compare its structure and electrical properties with the growth of these films on traditional Pt/TiO_2/SiO_2/Si (100) Si substrates. To our knowledge, no reports are available on the magnetoelectric coefficient dependence on the dc bias magnetic field of the *LFO-BFO* heterostructure deposited on conductive oxide with perovskite structure. The magnetic and dielectric properties of such thin films crystallized by the polymeric precursor method were investigated for being crucial for device engineering applications. The motivations are as follows: LSCO as a conduction layer and high oxygen affinity which avoids the migration of charge species for the electrode-film interface can be used to tailor the collective physical properties of the system.

2 Experimental procedure

The LSCO bottom electrode thin film were spin coated (KW-4B, Chemat Technology) on (100) Pt/Ti/SiO_2/Si substrates by a commercial spinner operating at 5000 revolutions/min for 30 s. Each annealing layer was pre-fired at 400 °C for 2 h in a conventional oven. After the pre-firing, each layer was crystallized in a conventional furnace under an oxygen flow of 50 cm^3/min at 800 °C for 1 h employing six layers. Using the same procedure, the *BFO-LFO* thin films were deposited by spinning the precursor solution on the desired substrates at 500 °C for 2 h employing 10 layers. In this case, each annealing layer was pre-fired at 300 °C for 1 h in a conventional oven. Phase analysis of the films was performed at room temperature from X-ray diffraction (XRD) patterns recorded on a Rigaku-DMax 2000PC with Cu-Kα radiation in the 2θ range from 20° to 60° with 0.3°/min steps. The Rietveld analysis was performed with the Rietveld refinement program DBWS-941 1. The profile function used was the modified Thompson-Cox-Hasting pseudo-Voigt, in which η (the lorentzian fraction of the function) varies with the Gauss and Lorentz components of the full width at half maximum. The

annealed thin film thickness was determined using scanning electron microscopy (SEM) (Topcom SM-300) by checking the cross- section where back-scattered electrons were utilized. Three measurements were taken to obtain an average thickness value. The surface morphology of thin films was measured by AFM using a tapping mode technique (Nanoscope IIIa-Bruker). Dielectric properties of the capacitor were measured with an HP4192A impedance/gain phase analyzer under zero bias for a film thickness of 364 and 356 nm for the heterostructures on Pt and LSCO respectively. The crystallite size (d) of the films was calculated using the Scherrer equation $d = k\lambda/\beta \cos\theta$, where k is a constant, λ is the wavelength of X- rays, and β is the full width at half maximum (FWHM) for maximum reflection measured from a slow scan where θ is the diffraction angle of the main peak.

A 0.5 mm diameter top Au electrode was sputtered through a shadow mask at room temperature. After deposition of the top electrode, the film was subjected to a post-annealing treatment in a tube furnace under an oxygen atmosphere at 300 °C for 1 h. Here, the desired effect was to eventually decrease present oxygen vacancies. The *J-V* measurements were recorded on the Radiant Technology tester in the current–voltage mode, with a voltage change from 0 to +10 V, from +10 to −10 V and back to 0 V. The hysteresis loop measurements were carried out on the films with a Radiant Technology RT6000HVS at a measured frequency of 60 Hz. These loops were traced using the Charge 5.0 program included in the software of the RT6000HVS in a virtual ground mode test device. The magnetoelectric coefficient measurements in the films were attained in a dynamic lock-in technique. Additionally, an ac magnetic field up to 10 Oe with frequency of 7 kHz was superimposed onto the dc field. The ac field was produced by a Helmholtz-type coil (180 turns witha diameter of 50 mm), driven by an ac current generated by a function generator (Philips PM5192). The amplitude of the ac field was calculated from the driving current measured by a multimeter (Keitley 196 System DMM). Films were located in the magnetic field with the surface perpendicular or parallel to the field direction, for longitudinal and transverse measurements, respectively. The dc magnetic bias field was produced by an electromagnet (Cenco Instruments J type). The time-varying dc field was achieved by a programmable dc power supply (Phillips PM2810 60 V/5 A/60 W). A Hall probe was employed to measure the dc magnetic field. Magnetization measurements were done by using a vibrating-sample magnetometer (VSM) from Quantum Design™. The magnetoelectric signal was measured by using a lock-in amplifier (EG&G model 5210) with input resistance and capacitance of 100 MΩ and 25 pF, respectively. Piezoelectric measurements were carried out using a setup based on an atomic force microscope in a Multimode Scanning Probe Microscope with Nanoscope IV controller (Veeco FPP-100). In our experiments, piezoresponse images of the films were acquired in ambient air by applying a small ac voltage with an amplitude of 2.5 V (peak to peak) and a frequency of 10 kHz while scanning the film surface. To apply the external voltage we used a standard gold coated Si_3N_4 cantilever with a spring constant of 0.09 N/m. The probing tip, with an apex radius of about 20 nm, was in mechanical contact with the uncoated film surface during the measurements. Cantilever vibration was detected using a conventional lock-in technique.

3 Results and discussion

From Fig. 1 we can see that the XRD patterns of the films are fully crystallized since extremely intense and thin peaks are evident and no impure phase such as $Bi_2Fe_4O_9$ and $Bi_{46}Fe_2O_{72}$ phases are observed, except for the Si (100) and Pt (111) peaks. According to the pattern, the film has a hexagonal perovskite structure. Furthermore, it is randomly oriented. As shown in Fig. 1, the strongest peak of the LSCO thin film corresponds to non-oriented LSCO (110) grains with perovskite structure being its position in the pattern coincident with the heterostructured thin films (012) orientation. It was found that all the films consisted of a single phase showing preferred (012) and (111) orientations. The origins of *c*-axis orientation is attributed to the self-oriented growth behavior resulted from rapid thermal processing and the {001} surface. The preferred orientation can be attributed to the small differences in nucleation energy between the ferroelectromagnetic material and the bottom electrode. The clear identification of these two

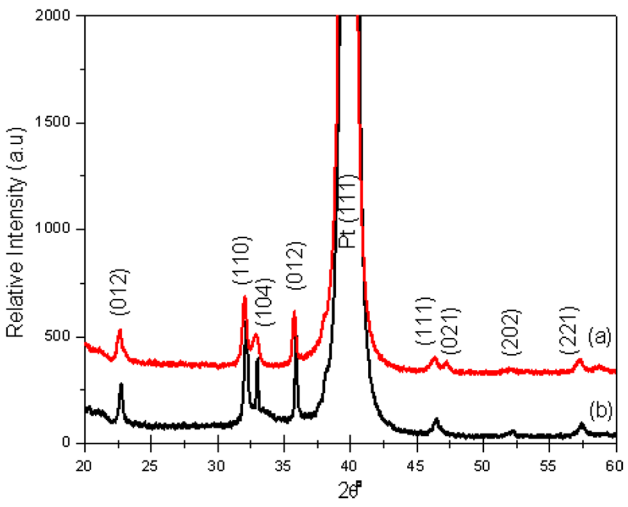

Fig. 1 X-ray diffraction of thin films deposited by the polymeric precursor method and annealed at 500 °C in static air for 2 h: (*a*) Pt and (*b*) LSCO

sets of peak groups without any secondary phase shows that there was little chemical reaction or diffusion between these two constituent layers. The crystal sizes of the phases involved were calculated using the Debye–Scherrer equation, which gave a crystal size of 54 nm for the heterostructured thin films deposited on LSCO bottom electrode and around 40 nm for the *BFO–LFO* layer on Pt. These results reveal that the crystal size of the heterostructure on Pt was smaller as compared to that of the sublayers on LSCO. The lattice parameters (*a* and *c*) and the unit cell volume (V) of the BFO layers are a (Å) = 5.6011 ± 0.5, c (Å) = 13.6429 ± 0.5 and V (Å^3) = 371.01 ± 0.5%. The atomic positions obtained by Rietveld analyses belong to the ICSD card (PDF # 71-2494) with hexagonal symmetry.

Figure 2a, b shows the SEM cross sectional images of the *BFO–LFO* heterostructure on different bottom electrodes. The SEM studies reveal a clear boundary between two different layers, indicating that the LFO sublayer was deposited on the top of the BFO sub layer. Substantial diffusion between two different phases was not observed, which is consistent, with the XRD phase analysis results. It is observed that the thicknesses of both films are very well-defined.

To confirm the surface morphology, *AFM* was carried out. The results are shown in Fig. 3. Changes on the surface morphology of the both films were evaluated. AFM studies revealed that independently of the bottom electrode homogeneous surface was observed indicating that the polymeric precursor method allows the preparation of films with controlled morphology. The average surface roughness value is 13 ± 2% nm for the film deposited on LSCO electrode and

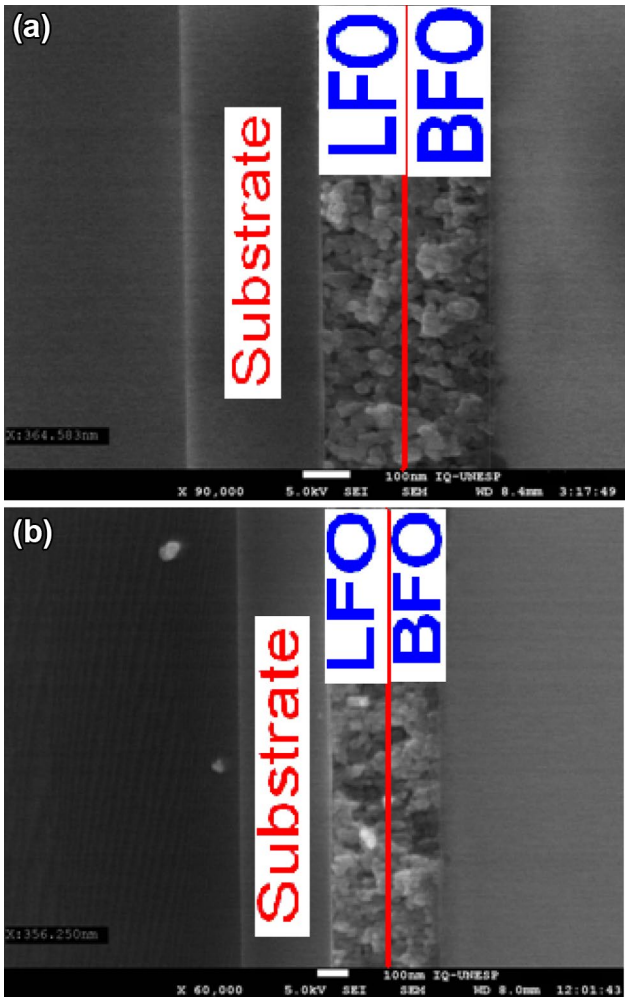

Fig. 2 Cross section of LFO/BFO. thin films deposited by the polymeric precursor method and annealed at 500 °C in static air for 2 h: **a** Pt and **b** LSCO

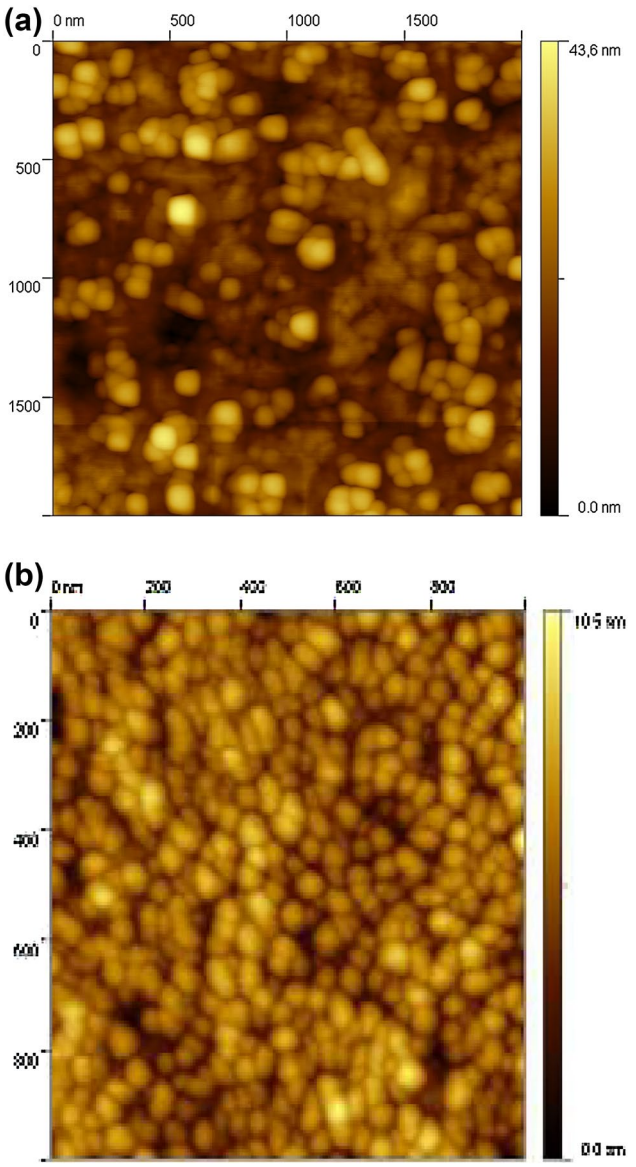

Fig. 3 AFM micrographies of thin films deposited by the polymeric precursor method and annealed at 500 °C in static air for 2 h: **a** Pt and **b** LSCO

17 ± 2% nm for the film deposited on Pt bottom electrode. The average grain size is 68 ± 4 and 85 nm ± 4, respectively. It was also found that the Pt electrode tends to suppress the grain growth. These results are consistent with the XRD results where a decrease in peak sharpness and intensity was observed with Pt electrode. The heterostructure deposited on Pt consists of grains with random size distribution with an average grain size of 68 nm (Fig. 3b). Figure 3a shows the *BFO–LFO* heterostructure thin films on LSCO which exhibit a huge grain size of 85 nm with less degree of porosity which indicates that the bottom electrode was able to promote the grain growth of the heterostructure during the annealing process. As expected, the surface roughness of the heterostructure on LSCO, which was nearly 13 nm, was smaller than that of the film deposited on Pt substrate. The role of oxide bottom electrode is to eliminate vacancies which act as point defects and therefore decrease the surface heterogeneity in the films. The decrease of grain size of the film deposited on Pt electrode can be interpreted by slower oxygen ion motion and consequently lower grain growth rate. In this way, the lower grain size can be a reflex of increase in crystallization temperature due to differences of chemical bond strength between Fe–O, La–O, Bi–O and Pt atoms.

Figure 4a, b shows frequency-dependent dielectric behavior of the *BFO–LFO* heterostructured film annealed at 500 °C on both bottom electrodes. The dielectric measurements were carried out at room temperature as a function of frequency in the range of 10–1 MHz. The films have a small dielectric dispersion at low frequency and the dielectric constants decrease slightly with the frequency, indicating that the films have a good interface with the bottom electrode. The dielectric constant shows very little dispersion with frequency indicating a low concentration of defects at the interface film-substrate. The low dispersion of the dielectric constant and the absence of any relaxation peak in tan δ indicate that both, the interfacial polarization of the Maxwell Wagner type and a polarization produced by the electrode barrier can be neglected in the film measurements. The dielectric constant and dissipation factor, at 100 kHz, were found to be 307 and 0.05, respectively for the film deposited on Pt (Fig. 4a), 400 and 0.04 for the film deposited on LSCO. The heterostrutured film had a smaller relative dielectric permittivity (400) when compared with those previously reported in ceramics or films [29–34]. The observed improvement in the dielectric permittivity on LSCO may be associated with higher structural disorder and two-dimensional stress in the plane of the film. The tan δ values of the *BFO–LFO* films changed with increasing frequency suggesting that the films exhibited space charges in low concentration in the sublayers. The tangent loss of the heterostructure is 0.03 and stabilizes after a certain frequency indicating that space charges and defects associated

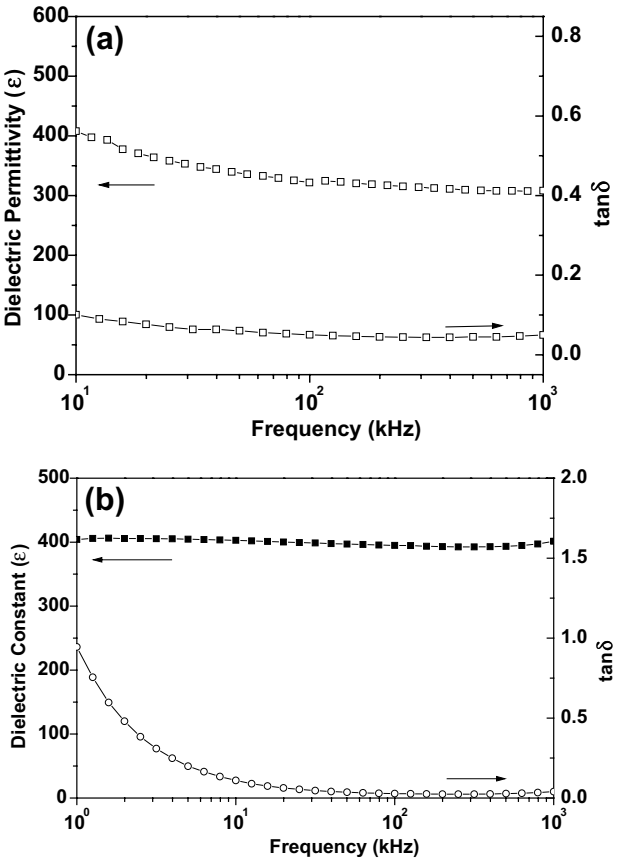

Fig. 4 Dielectric permittivity and dielectric loss spectra as a function of frequency of thin films deposited by the polymeric precursor method and annealed at 500 °C in static air for 2 h: **a** Pt and **b** LSCO

with interfaces have effect in the interface due the improvement in the dielectric permittivity. The variation in dielectric loss is attributed to the difference in leakage and decrease in insulating *BFO-LFO* grain boundaries. Based on the analysis of the dielectric properties it is observed that the conductivity of the films increases on Pt substrate, which is attributed to the increase in semiconducting grains and decrease in insulated *BFO-LFO* grain boundary. As the grain boundary is reducing, in turn the hopping barrier for the trapped carriers decreasing, more polarons have sufficient energy to jump over the barrier or to get along hopping length.

Figure 5 shows the leakage currents density as a function of voltage measured at room temperature. The curve was recorded with a voltage step width of 0.1 V and elapsed time of 1.0 s for each voltage. The measured logarithmic current density (log J) versus the voltage (V) is symmetric and shows two clearly different regions. The insulating properties of the films were found to be dependent on the bottom electrode. The leakage current density decreased for the films deposited on LSCO bottom electrode. Such a reduction in leakage current density may be attributed to

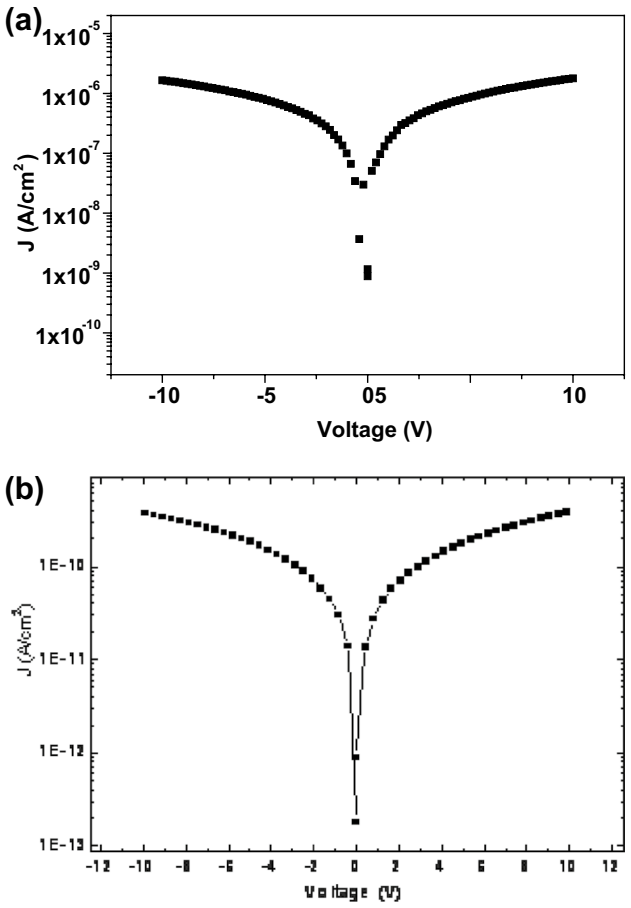

Fig. 5 Leakage current density versus applied voltage of thin films deposited by the polymeric precursor method and annealed at 500 °C in static air for 2 h: **a** Pt and **b** LSCO

high oxygen affinity of the LSCO bottom electrode avoiding that oxygen in the electrode material will be depleted by the ferroelectric material, thus leaving an oxygen deficient layer of the electrode at the interface and increasing the contact resistance. From this study it can be demonstrated that the microstructures of ferroelectric films play an important role in their conductivity properties. Such a reduction in leakage current density may be attributed to reduction of the number of electrons injected from the cathode at a rate faster than they can travel through the film. A low threshold electric field was applied in order to overcome the larger repulsion forces that are due to an increase amount of non-neutralized charges in the traps of the LFO film. This study demonstrates that the microstructures of ferroelectric films play an important role in their conductivity properties [35]. Since the conductivity is strongly affected by the characteristics of the film-electrode interface, the lower leakage current observed here may be probably attributed to differences in grain size, density, and less stress in the plane of the film due to differences in the ferroelectric material and the interface. The current density increases linearly with the external voltage in the region of low applied voltage strengths which suggests an ohmic conduction. At higher field strengths, the current density increases exponentially which implies that at least one part of the conductivity results from the Schottky or Poole–Frenkel emission mechanism. The leakage current density at 5.0 V changes from 10 to 10 (LSCO) to 10^{-7} A/cm^2 (Pt). The main reason for such a small value can be attributed to changes in the surface roughness and the reduction of microcracks due to modification on the interface stability on oxide electrode. Thus, LSCO bottom electrode reduces oxygen vacancies improving switching process of ferroelectric domains. Other reason for this is that introduction of Pt as a bottom electrode reduces grain sizes of the film as evidenced by *AFM*, leading to an increase in the density of grain boundaries, which makes contribution to the decreased leakage current density [27]. Normally, the mobile oxygen vacancies are donor like trapping centers for electrons. The energy levels associated with $(V_{O2-})^{\cdot\cdot}$ are very close to the conduction band. Therefore, the electrons can be readily activated to be free for conduction by the electric field. However, the electric field required for generating the free electrons in BFO-based film may be increased if the defect complexes between the $(V_{O2-})^{\cdot\cdot}$ are formed, since the applied electric field has to overcome the electrostatic attraction force between $(V_{O2-})^{\cdot\cdot}$ and (V_{Bi}''') before the oxygen vacancies become mobile and can serve as the trapping centers for electrons. Note that the different positions occupied by $(V_{O2-})^{\cdot\cdot}$ in perovskite octahedral will result in different electrostatic forces between (V_{Bi}''') and $(V_{O2-})^{\cdot\cdot}$, which in turn lead to that the different electric fields will be required for breaking the defect complexes. Based on the above discussion, the high leakage current in LFO-BFO film deposited on Pt compared to that deposited on LSCO may result from the formation of defect complexes between (V_{Bi}''') and $(V_{O2-})^{\cdot\cdot}$. Thus, the increase of the leakage current with the electric field can be ascribed to the gradual release of $(V_{O2-})^{\cdot\cdot}$ from the complexes of (V_{Bi}''')–$(V_{O2-})^{\cdot\cdot}$.

The room temperature *P-E* hysteresis loops of *BFO-LFO* films deposited on Pt and LSCO electrodes are shown in Fig. 6a, b. No sign of leakage has been observed under a measuring frequency of 60 Hz. Possibly, low coercive fields could be expected as the bottom BFO sublayer was subjected for a longer annealing time period resulting in a higher concentration of defects and higher leakage. For that reason, a couple of films were prepared on LSCO bottom oxide electrodes to minimize formation of oxygen vacancies between the sublayers. The projection polarization along the (110) orientation is larger than the polarization of the (100) orientation. The *P-E* hysteresis loop of the *BFO-LFO* layer on Pt shows a *P*r of 52 μC/cm^2 after applying

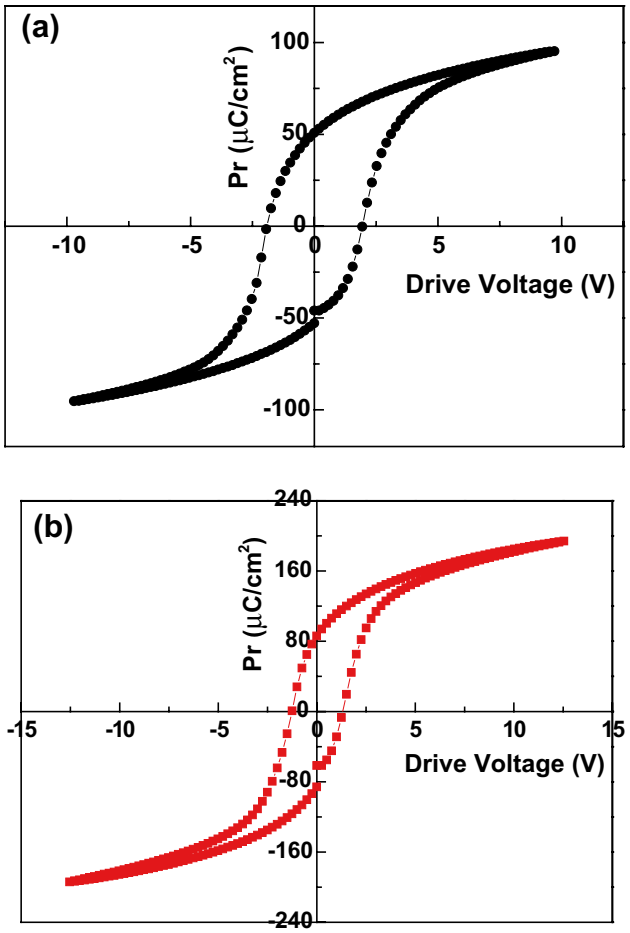

Fig. 6 Hysteresis loop of thin films deposited by the polymeric precursor method and annealed at 500 °C in static air for 2 h: **a** Pt and **b** LSCO

a voltage of 10 V. These high values are not intrinsic, but are induced by high leakage in this structure, as indicated by the roundish shape of the *P-E* loop. Additionally, space charges can also contribute to the polarization property. The loop deposited on LSCO bottom electrode is well saturated and rectangular with a *Pr*~80 μC/cm^2 after applying a voltage of 12 V. Since our films are intense (111) we reasonably expect a larger polarization on LSCO bottom electrode. A moderate coercive field probably originates from the intermediary grain size (85 nm) of the *LFO*/*BFO* layer deposited on LSCO electrode. However, for the film deposited on Pt electrode the trapped charge (O_2'') associated with other defects ($V_0^{\cdot\cdot}$) or even defect dipole complexes such as oxygen vacancies associated to bismuth vacancies (V'''_{Bi}–$V_0^{\cdot\cdot}$) located in the grain boundary and in the film-electrode interface can promote a local stoichiometry deviation influencing the shape of the hysteresis loops. As a consequence of these space charges, a significant shift along the electric field axis towards the positive bias, which is defined as imprint, may lead to a failure of the capacitor. A more symmetric hysteresis loop is observed for the film deposited on LSCO electrode indicating that the high oxygen affinity of this material avoids the migration of charge species to the electrode-film interface. This behavior can be ascribed to the larger grains of the bilayered thin films deposited on LSCO bottom electrode. The domain walls in larger grains are easier to be switched under external field. Similar phenomena have been found in $SrBi_2Ta_2O_9$ and $PbTiO_3$ thin films [36, 37]. The polarization switching in films with small grains is usually more difficult, as in the case of Pt electrode. Therefore, the growth of the film in one direction not coincident to *c*-axis preferred orientation will favor larger grains morphology, such as the ones grown on LSCO bottom electrode leading to a lower drive voltage when compared to those grown on Pt. The *BFO-LFO* layer deposited on Pt electrode exhibits a poor *P–E* hysteresis loop, which has been typically observed from conductive ferroelectrics and it get breakdown with increased bias electric field due to a large leakage current. The *BFO-LFO* ferroelectric properties may be related to decreased grain size with Pt electrode, since the strength of polarization is strongly related to the grain size [38]. It has been found that the polarizability in perovskites (ABO_3) is partially related with the sizes of A and B cations. In general, a large A cation results in an increase in polarizability, since the large A cation leads to "a larger rattling space" available for B cation by increasing the size of the oxygen octahedron. The increased remnant polarization of LFO/BFO layer on LSCO bottom electrode can be explained by the inhibition of defect complexes between (V_{Bi}''') and $(V_{O2-})^{\cdot\cdot}$. In the case of the film deposited on Pt electrode, the decreased volume fraction of dielectric polarization with decreasing grain size could have predominant effect on the remnant polarization.

Magnetizations (M) versus field (H) loops were recorded at 300 K (Fig. 7a, b). The magnetic hysteresis loops of the *BFO-LFO* heterostructure deposited on both bottom electrodes is presented. All films exhibit hysteresis loops with a saturation magnetization of 4.6 and 2.5 emu/g, respectively. The ferromagnetic response suggests that the magnetic behavior is influenced by the crystal size as M_s has been reported to drop according with the reduction in the crystal size [39, 40]. The coercive fields (Hc) are 0.014 and 0.019 kOe, respectively. The possible origins of the difference in the magnetic properties are mainly attributed to distinct factors. One is the variation of grain size. As it is well known, the particle size has been reported to influence the magnetic properties of the materials. Here, the crystallite sizes of all the LFO-BFO films are below 62 nm, where the spiral spin structure is destroyed, which will lead to the uncompensated spins existence at the crystallite surface, in turn result in the appearance of the uncompensated spins

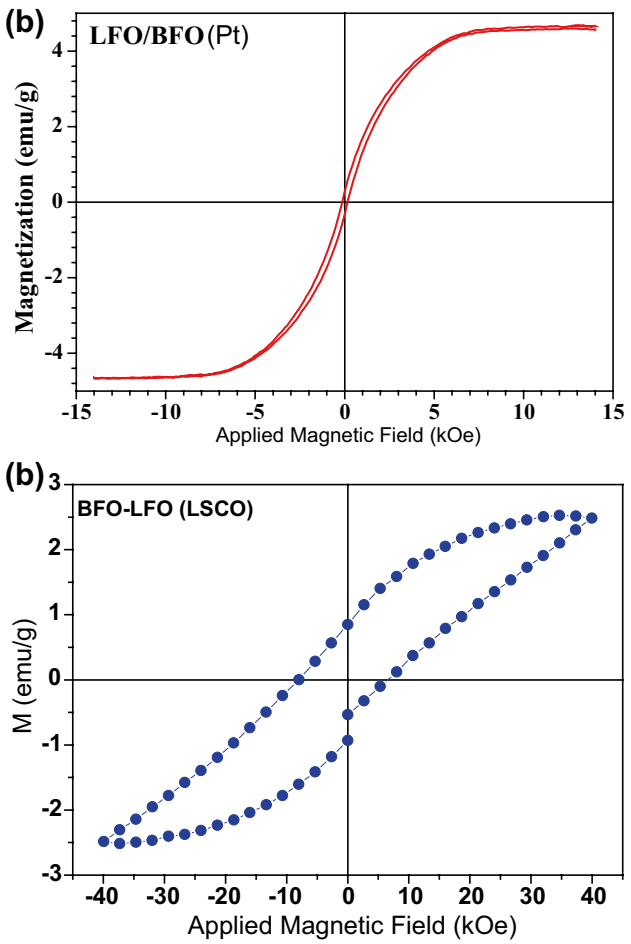

Fig. 7 Field dependencies of the magnetization obtained of thin films deposited by the polymeric precursor method and annealed at 500 °C in static air for 2 h: **a** Pt and **b** LSCO

at the grain boundary [41]. Additionally, the effect of texture difference resulting from magnetic annealing should be considered. Other possible reasons for this enhancement in magnetization: (i) the spatial homogenization of the spin arrangement [42]; (ii) the distorted spin cycloid structure when LSCO is introduced as bottom electrode [43]; (iii) the formation of partial Fe^{2+}; (iv) the varied canting angle of the Fe–O–Fe bond [44]; or (v) the increased tensile strain changing the balance between the antiferromagnetic and ferromagnetic interactions [45]. However, the magnetization difference observed in the above films may not be attributed to the crystallite size since all the crystallites have almost the same size, as shown in Fig. 1. Nevertheless, with decrease in the grain boundary due to increasing the applied annealing field, the uncompensated spins at the grain surface reduce. As a result, the magnetization of the fields-annealing heterostructured thin films is lower than the non-field-annealing one. The other factor is the degree of the crystallite rotation and alignment along the annealing field direction. Applying magnetic field during the annealing process can improve the connection and diffusion of components as well as rotating the crystals to align along the annealing field direction [45]. Such rotation and alignment of the crystallites result in enhancement of magnetization. Generally, decreasing uncompensated spins at the grain boundary and increasing alignment degree of the BFO crystallites with increasing annealing field lead to the magnetization and the magnetic interaction between different grains decreasing initially, and then increasing, which further results in the same variation of the spin-glass transition temperature [46]. Since LSCO bottom electrode result in better magnetic response, it is consequently to believe that if oxygen vacancy accumulation near the film-electrode interface occurs during measurement, the conductive oxide can provide the oxygen to those vacancies by changing their oxygen nonstoichiometry and thus, the accumulation of oxygen vacancies near the interface is prevented or reduced. On the other hand, films deposited on Pt electrode reveal an increase in local current around the nucleation sites which can damage the film-electrode interface and suppress the nucleation of oppositely oriented domains at the surface. The LSCO bottom electrode can maintain the stability of the interface and bulk defects and solve the weak ferromagnetism of bilayered thin films. On the other hand, the film deposited on Pt can provide conductive electrons which reduce the polarization and increase the concentration of holes in the interface region. The marked improvement in the fatigue behavior of LSCO bottom electrode may result from the crystallinity, electrode /ferroelectric interface, and defect concentration.

The magnetolectric coefficient versus dc bias magnetic field in the longitudinal and transversal directions reveals hysteretic behavior, as observed in the magnetic field cycles shown in Fig. 8a–d, for Pt and LSCO respectively. The maximum magnetoelectric coefficient of 12 V/cmOe in the longitudinal direction is much larger than that previously reported for thin films which was as high as 3 V/cmOe in the same direction at zero fields [47] which is a consequence of the antiferromagnetic axis of *BFO-LFO* which rotates through the crystal with an incommensurate long-wavelength period of ~620 Å [48, 49]. Early reports showed that the spiral spin structure leads to a cancellation of any macroscopic magnetization and would inhibit the observation of the linear magnetoelectric effect [50]. The hysteretic behavior with peaks at 0.5 kOe comes from the Hc of films being the maximum magnetoelectric coefficient observed when the maximum linear magnetostriction appears. Upon changing the measuring conditions from longitudinal to transverse, H_{max} changes due to the different demagnetizing field. Significant magnetization (~0.5 μ*B*/unitcell) and a strong magnetoelectric coupling have been observed in epitaxial thin films, suggesting that the spiral spin structure

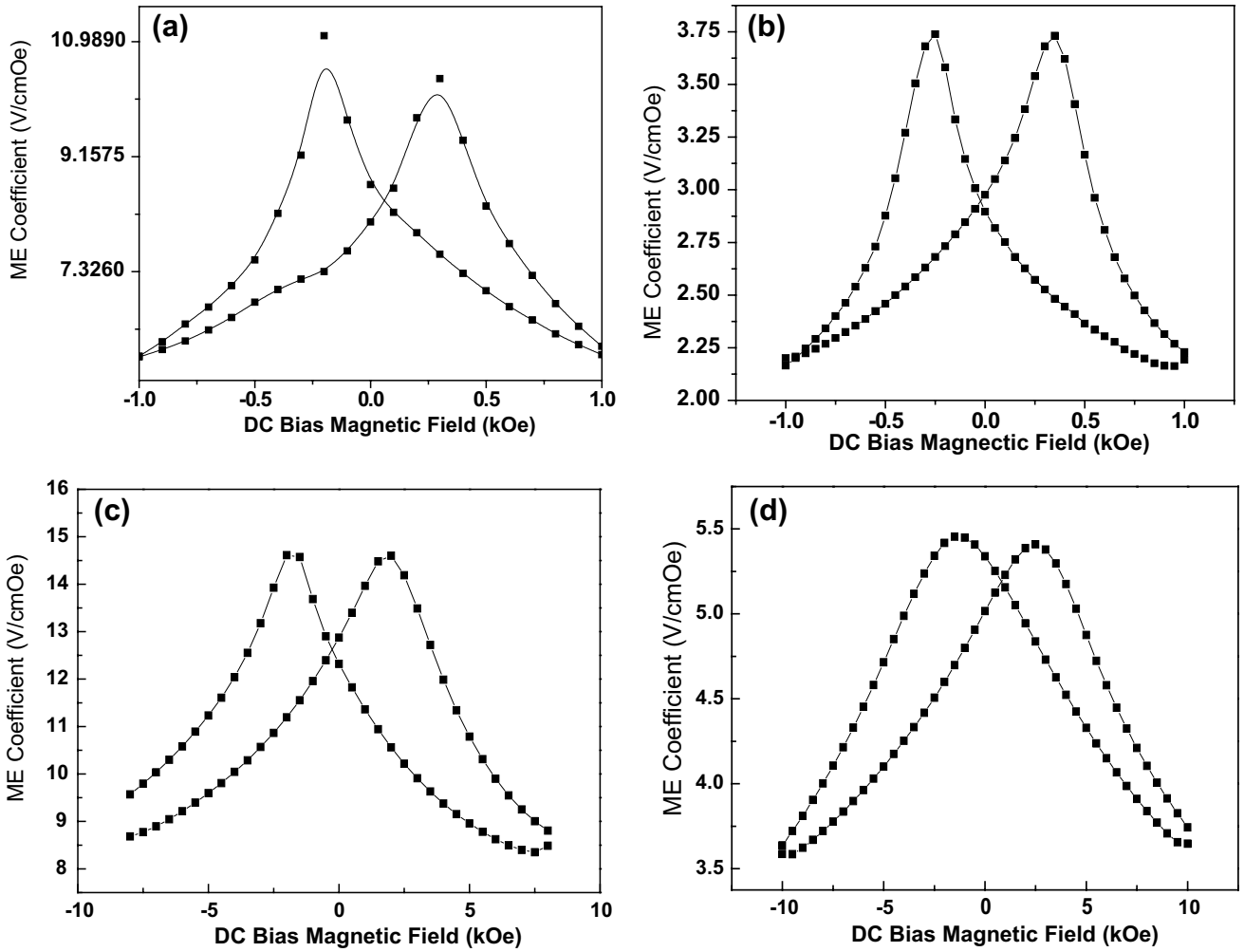

Fig. 8 The magnetoelectric coefficient dependence on dc bias magnetic field on Longitudinal (L) and Transversal (T) directions for LFO-BFO thin films deposited by the polymeric precursor method and annealed at 500 °C in static air for 2 h: **a** Pt (L), **b** Pt (T), **c** LSCO (L) and **d** LSCO (T)

could be suppressed [51]. Due the huge grains presented in the *BFO-LFO* heterostructure on LSCO electrode a significant enhance of magnetoelectric coefficient (14 V/cmOe in the longitudinal direction and 5.3 in the transversal direction) was observed which suggest that the *AFM* domains serve to pin an adjacent ferromagnetic (FM) layer by force of the exchange-bias coupling in such compound. Also, $BiFeO_3$ and $LaFeO_3$ are G-type *AFM* with comparable Fe magnetic moments (3.75 and 4.6 μB respectively) and high Neel temperatures (643 and 750 K, respectively). Hence, a similar magnetic order well above room temperature was observed. Both materials have a strong tendency to similar crystal structure distortion which in turn is compatible with coupling of lattice modes.

To visualize the domain structures of the heterostructures thin films, we performed piezoelectric force microscopy (*PFM*) and the results are illustrated in Fig. 9. The out-of-plane (*OP*) and in-plane (*IP*) piezoresponse images of the as-grown films after applying a bias of −12V, on an area of 2 x 2 μm, and then an opposite bias of +12 V in the central 1 x 1 μm area were employed. To obtain the domain images of the films, a high voltage that exceeds the coercive field was applied during scanning. The contrast in these images is associated with the direction of the polarization [52]. Topography is illustrated in Fig. 9a, d. The white regions in the out-of-plane *PFM* images correspond to domains with the polarization vector oriented toward the bottom electrode hereafter referred to as down polarization (Fig. 9b, e) while the dark regions correspond to domains oriented upward referred to as up polarization. Grains which exhibit no contrast change are associated with zero out-of-plane polarization. A similar behavior was observed when a positive bias was applied to the film. We noticed that some of the grains exhibit a white contrast associated

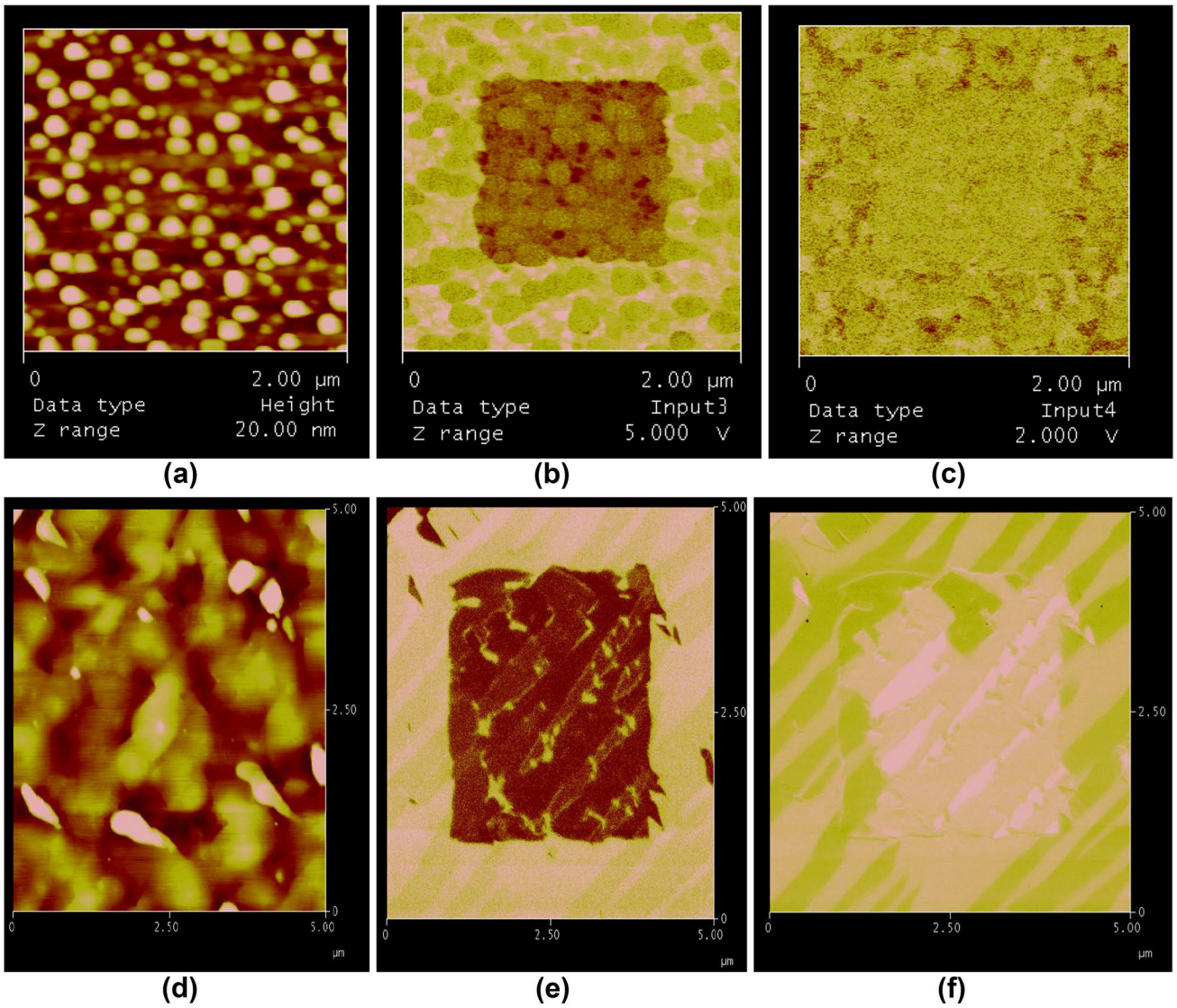

Fig. 9 Piezoresponse microscopy obtained of thin films deposited by the polymeric precursor method and annealed at 500 °C in static air for 2 h: **a** topography; **b** out-of-plane and **c** in-plane on Pt and **d** topography; **e** out-of-plane and **f** in-plane on LSCO

to a component of the polarization pointing toward the bottom electrode. On the other hand, in the in-plane PFM images (Fig. 9c, f) the contrast changes were associated with changes of the in-plane polarization components. In this case, the white contrast indicates polarization e.g. in the positive direction of the y-axis while dark contrast are given by in-plane polarization components pointing to the negative part of the y-axis. The ferroelectric domains of our films consist of a multiple domain state in a mixture of 71° and 180° domains which grow large into blocks. That the domains grow in multiple states is the consequence of thickness of films being close to 300 nm. *PFM* measurements reveal a clear piezoelectric contrast corresponding to antiparallel domains on all locations tested. Local piezoresponse is approximately two times weaker as compared with undoped $BiFeO_3$ ceramics, [53] pointing out a smaller value of the spontaneous polarization. There is no reduction in the amplitude of the measured vibrations for the highest doped film which is indicative that this phase is still polar and electric field-induced polarization switching still exists. Therefore, our data confirm that the spontaneous polarization is very high with addition of LFO sublayer. In this way, the LFO sublayer can reduce the strain energy and pin charged defects. This is a consequence of changes in grain boundary resistance for the multi-layered films which suggest low conductivity. In this way, lanthanum ferrite sublayer reduces the oxygen vacancies and as consequence improves the switching process of electrical dipoles. Pure BFO present defects as Bi or Fe vacancies resulting in an increase in conductivity. Therefore, this fact

indicates the presence of mobile carriers which are positively charged and that the possibility of hopping through the Bi ion can be considered. Also, we noted that some of the crystallites apparently have not been switched and still exhibit a positive piezoresponse signal. This result, which can be explained by strong domain pinning in these crystallites, is direct experimental proof that repeated switching results information of unswitchable polarization, which, in turn, leads to the degradation of switching characteristics. The presence of LSCO as bottom electrode is effective in controlling the volatility of Bi atoms in order to suppress oxygen vacancy concentration since the energy of the La–O bond (789.6 ± 8 kJ mol^{-1}) is stronger than that of Bi–O bond (337.2 ± 12 kJ mol^{-1}) [52, 54, 55]. The root mean square roughness values are 17 and 13 nm for *BFO-LFO* in Pt and LSCO, respectively, indicating that oxide electrode can also smooth the film surface morphology. The ferroelectric domain structures of the *BFO-LFO* on Pt exhibit a domain size similar to the grain size and upward or downward polarization within each domain (Fig. 9b). The domain structures of the *BFO-LFO* on LSCO show more homogeneous domains and the domains are pinned at the ground boundaries (Fig. 9e). The density of the domain walls in the *BFO-LFO* on LSCO is less than in the BFO; therefore, it is expected that there is a lower leakage of current in the *BFO-LFO* on LSCO since certain domain walls in the *BFO-LFO* on Pt are much more conductive than the domains themselves [53]. There exist three types of domain walls, namely those that separate domains 71°, 109° and 180° different in polarization [56]. Domain patterns can develop with either a {1 0 0}-type plane for 109° walls or a {1 0 1}- type plane for 71° walls, respectively [57]. As shown from the XRD spectra, the polycrystalline films should be a mixture of all three types of domain wall. The domain size in the *BFO-LFO* on LSCO film is larger than that in the Pt, which could originate from the tensile strain enhanced by the bottom electrode, the bigger grain size or even the misfit dislocation between the film and the substrate [58]. The domain structure and the density of the domain walls of the *BFO-LFO* on LSCO also suggests that it can undergo a higher electric bias and is easier to polarize than the *BFO-LFO* on Pt.

4 Conclusions

A *BFO-LFO* heterostructure has been created by a chemical solution deposition method with magnetocoupling and no secondary phases being found. The heterostructure shows a *P*r of μC/cm^2 after applying a voltage of 12 V. Structural defects as high porosity are responsible for the high leakage of the *BFO-LFO* heterostructure on Pt. The high dielectric permittivity of the *BFO-LFO* on LSCO was mainly due to less structural disorder and less two-dimensional stress in the plane of the film. In-plane magnetization-field curves revealed improvement of magnetization of the heterostructure which was influenced by the crystal size. The maximum magnetoelectric coefficient was nearly 14 V/cmOe in the longitudinal direction for the *BFO-LFO* film on LSCO. A remarkable improvement in the drive voltage suggest that *BFO-LFO* film on LSCO electrode is suitable for integrated device applications whereas a multiferroic state combining ferroelectricity and weak ferromagnetism is observed. The presented results suggest that such system is a promising candidate to achieve electric switching of the magnetization at room temperature. We hope that this work will motivate further experimental investigations.

Acknowledgements The financial support of this research project was from the Brazilian research funding agencies CNPq 573636/2008-7, INCTMN 2008/57872-1 and FAPESP 2013/07296-2. We would like to thank CMDF for facilities.

References

1. N.A. Spaldin, M. Fiebig, The renaissance of magnetoelectric multiferroics. Science. **309**(5733), 391–392 (2005)
2. M. Fiebig, T. Lottermoser, D. Fröhlich, A.V. Goltsev, R.V. Pisarev, Observation of coupled magnetic and electric domains. Nature. 419(6909), 818–820 (2002)
3. N. Ikeda, H. Ohsumi, K. Ohwada, K. Ishii, T. Inami, K. Kakurai, Y. Murakami, K. Yoshii, S. Mori, Y. Horibe, H. Kito, Ferroelectricity from iron valence ordering in the charge-frustrated system $LuFe_2O_4$. Nature. **436**(25), 1136–1138 (2005)
4. J. Wang, J.B. Neaton, H. Zheng, V. Nagarajan, S.B. Ogale, B. Liu, D. Viehland, V. Vaithyanathan, D.G. Schlom, U.V. Waghmare, N.A. Spaldin, K.M. Rabe, M. Wuttig, R. Ramesh, Epitaxial $BiFeO_3$ multiferroic thin film heterostructures. Science. **299**(5613), (2003) 1719–1722.
5. M. Gajek, M. Bibes, S. Fusil, K. Bouzehouane, J. Fontcuberta, A. Barthélémy, A. Fert, Tunnel junctions with multiferroic barriers. Nature Mater. **6**(4), 296–302 (2007)
6. F. Kubel, H. Schmid, Structure of a ferroelectric and ferroelastic monodomain crystal of the perovskite $BiFeO_3$. Acta Crystallogr. Sect. B **46**(6), 698–702 (1990)
7. S.V. Kiselev, R.P. Ozerov, G.S. Zhdanov, Detection of magnetic order in ferroelectric $BiFeO_3$ by neutron diffraction. So Phys. Dokl. **7**(1), 742–744 (1962)
8. Y.H. Lee, J.M. Wu, Y.L. Chueh, L.J. Chou, Low temperature growth and interface characterization of $BiFeO_3$ thin films with reduced leakage current. Appl. Phys. Lett. **87**(17), 172901–172903 (2005)
9. P. Royen, K. Swars, Das System Wismutoxyd-Eisenoxyd im Bereich von 0 bis 55 Mol% Eisenoxyd. Angew. Chem. **69**(24), 779–782 (1957)
10. I. Sosnowska, T. Peterlin-Neumaier, E. Steichele, Spiral magnetic ordering in bismuth ferrite. J. Phys. C. Solid State Phys. **15**(23), 4835–4840 (1982)
11. J.G. Wu, G.Q. Kang, H.J. Liu, J. Wang, Ferromagnetic, ferroelectric, and fatigue behavior of (111)-oriented $BiFeO_3$/$(Bi_{1/2}Na_{1/2})TiO_3$ lead-free bilayered thin films. Appl. Phys. Lett. **94**(17), 172906–172908 (2009)

12. J.G. Wu, G.Q. Kang, J. Wang, Electrical behavior and oxygen vacancies in $BiFeO_3/[(Bi_{1/2}Na_{1/2})_{0.94}Ba_{0.06}]TiO_3$ thin film. Appl. Phys. Lett **95**(1), 192901–192903 (2009)
13. H. Béa, M. Bibes, S. Fusil, K. Bouzehouane, E. Jacquet, K. Rode, P. Bencok, A. Barthélémy, Investigation on the origin of the magnetic moment of $BiFeO_3$ thin films by advanced X-ray characterizations. Phys. Rev. B **74**(2), 020101 (2006).
14. D. Xie, Y. Zang, Y. Luo, X. Han, T. Ren, L. Liu, Structural, ferroelectric, dielectric, and magnetic properties of $BiFeO_3/Bi_{3.15}Nd_{0.85}Ti_3O_{12}$ multilayer films derived by chemical solution deposition. J. Appl. Phys. **105**(8), 084109 (2009).
15. E. Traversa, S. Matsushuma, G. Okada, Y. Sadaoka, Y. Sakai, K. Watanabe, NO_2 sensitive $LaFeO_3$ thin-films prepared by RF-Sputtering. Sens. Actuat. B-Chem. **24**(1), 661–664 (1995)
16. N.N. Toan, S.Saukko, Lantto SV, Gas sensing with semiconducting perovskite oxide $LaFeO_3$. Phys. B. **327**(2–4), 279–282 (2003)
17. D. Kuscer, M. Hrovat, J. Holc, S. Bernik, D. Kolar, Some characteristics of $A1_20_3$- and CaO-modified $LaFeO_3$-based cathode materials for solid oxide fuel cells. J. Power Sour. **61**(1), 161–165 (1996)
18. R. Dogra, A.C. Junqueira, R.N. Saxena, A.W. Carbonari, J.M. Filho, M. Moralles, Hyperfine interaction measurements in $LaCrO_3$ and $LaFeO_3$ perovskites using perturbed angular correlation spectroscopy. Phys. Rev. B **63**(2), 224104 (2001)
19. A. Scholl, J. Stohr, J. Luning, J.W. Seo, J. Fompeyrine, H. Siegwart, J.P. Locquet, F. Nolting, S. Anders, E.E. Fullerton, M.R. Scheinfein, H.A. Padmore, Observation of antiferromagnetic domains in epitaxial thin films. Science **287**(1), 1014–1018 (2000).
20. J. Nogues, I.K. Schuller, Exchange bias. J. Magn. Magn. Mater. **192**(2), 203–232 (1999).
21. J. Lu, D.A. Pan, L. Qiao, Inductance–capacitance resonance effect in the magnetoelectric composites characterization system. Appl. Phys. A Sept. **100**(4), 1069–1072 (2010)
22. E. Folven, T. Tybell, A. Scholl, A. Young, S.T. Retterer, Y. Takamura, J.K. Grepstad, Antiferromagnetic domain reconfiguration in embedded $LaFeO_3$ thin film nanostructures. Nano Lett. **10**(11), 4578–4583 (2010)
23. A.M. Dhote, S. Madhukar, W. Wei, T. Venkatesan, R. Ramesh, C.M. Cotell, Direct integration of ferroelectric La–Sr–Co–O/Pb–Nb–Zr–Ti–O/La–Sr–Co–O capacitors on silicon with conducting barrier layers. Appl. Phys. Lett **68**(10), 1350–1352 (1996)
24. K.S. Hwang, Y.M. Lee, S.S. Min, B.A. Kang, Epitaxially grown LaSrCoO3 thin films on various substrates by the Sol-Gel method. J. Sol-Gel Sci. Tech. **18**(2), 175–180 (2000)
25. K. Hwang, T. Manabe, I. Yamaguchi, S. Mizuta, T. Kumagai, Preparation of epitaxial $Pb(Zr,Ti)O_3$ thin films on MgO(100) substrates by dipping-pyrolysis process. J. Ceram. Soc. Jpn. **105**(1) 952–956 (1997)
26. K.H. Wong, W. Wu, P.W. Chan, J.T. Cheung, Low temperature growth of epitaxial LSCO films on (100) STO by pulsed laser deposition. Thin Solid Films **312**(2), 7–10 (1998)
27. V. Nagaraj, S. Aggarwal, R. Ramesh, Role of substrate on the dielectric and piezoelectric behavior of epitaxial lead magnesium niobate-lead titanate relaxor thin films. Appl. Phys. Lett **77**(3), 438–440 (2000)
28. M.S. Chen, T.B. Wu, J.M. Wu, Effect of Reducing atmosphere on electrical properties of sol–gel-derived $Pb(Zr,Ti)O_3$ ferroelectric films on textured $LaNiO_3$ electrode. Jpn. J. Appl. Phys **40**(1), 6045–6048 (2001)
29. M.M. Kumar, V.R. Palkar, K. Srinivas, S.V. Suryanarayana, Ferroelectricity in a pure $BiFeO_3$ ceramic. Appl. Phys. Lett. **76**(19), 2764–2766 (2000)
30. J.K. Kim, S.S. Kim, W. Kim, Sol–gel synthesis and properties of multiferroic $BiFeO_3$. J. Mater. Lett. **59**(29), 4006–4009 (2005)
31. H. Liu, Z. Liu, Q. Liu, K. Yao, Ferroelectric properties of $BiFeO_3$ films grown by sol–gel process. Thin Solid Films. **500**(1–2), 105–109 (2006)
32. V.R. Palkar, J. John, R. Pinto, Observation of saturated polarization and dielectric anomaly in magnetoelectric $BiFeO_3$ thin films. Appl. Phys. Lett. **80**(9), 1628–1630 (2002)
33. A.K. Pradhan, K. Zhang, D. Hunter, J.B. Dadson, G.B. Loutts, P. Bhattacharya, R. Katiyar, J. Zhang, Y. Sellmyer, A. Burger, Magnetic and electrical properties of single-phase multiferroic $BiFeO_3$. J. Appl. Phys. **97**(1), 093903–093906 (2005)
34. G.L. Yuan, S.W. Or, Y.P. Wang, Z.G. Liu, J.M. Liu, Preparation and multi-properties of insulated single-phase $BiFeO_3$ ceramics. Solid State Commun. **138**(2), 76–81 (2006)
35. J.K. Kim, S.S. Kim, S.W. Kim, Substitution effects on the ferroelectric properties of $BiFeO_3$ thin films prepared by chemical solution deposition. J. Appl. Phys. **101**(1), 014108–014110 (2007)
36. T. Li, Y. Zhu, S.B. Desu, C.H. Peng, M. Nagata, Metalorganic chemical vapor deposition of ferroelectric $SrBi_2Ta_2O_9$ thin films. Appl. Phys. Lett. **68**(5), 616–618 (1996)
37. A.L. Kholkin, V.V. Shvartsman, Y.A. Emelyanov, R. Poyato, M.L. Calzada, L. Pardo, Stress-induced suppression of piezoelectric properties in $PbTiO_3$:La thin films via scanning force microscopy. Appl. Phys. Lett. **82**(13), 2127–2129 (2003)
38. Y. Shimakawa, Y. Kubo, Y. Tauchi, H. Asano, T. Kamiyama, F. Izumi, Z. Hiroi, Crystal and electronic structures of $Bi_{4-x}La_xTi_3O_{12}$ ferroelectric materials. Appl. Phys. Lett. **79**(17), 2791–2793 (2001)
39. M.M. Kumar, S. Srinath, G.S. Kumar, Spontaneous magnetic moment in $BiFeO_3$ - $BaTiO_3$ solid solutions at low temperatures. J. Magn. Magn. Mater. **188**(1–2), 203–211 (1998)
40. C.S. Liang, J.M. Wu, M.C. Chang, Ferroelectric $BaPbO_3/PbZr_{0.53}Ti_{0.47}/BaPbO_3$ heterostructures. Appl. Phys. Lett. **81**(21), 3624–3626 (2002)
41. T.J. Park, G.C. Papaefthymiou, A. Viesca, A.R. Moodenbaugh, S.S. Wong, Size-dependent magnetic properties of single-crystalline multiferroic $BiFeO_3$ nanoparticles. Nano Lett. **7**(3), 766–772 (2007)
42. D. Lee, M.G. Kim, S. Ryu, H.M. Jang, S.G. Lee, Epitaxially grown La-modified $BiFeO_3$ magnetoferroelectric thin films. Appl. Phys. Lett. **86**(22), 222903–222905 (2005)
43. Y.H. Lee, J.M. Wu C.H. Lai, Influence of La doping in multiferroic properties of BiFeO3 thin films. Appl. Phys. Lett. **88**(1), 042903–042905 (2006)
44. C.J.M. Daumont, D. Mannix, S. Venkatesan, G. Catalan, D. Rubi, B.J. Kooi, J.T.M.D. Hosson, B. Noheda, Epitaxial TbMnO3 thin films on $SrTiO_3$ substrates: a structural study. J. Phys Mater. **21**(1), 182001–182005 (2009)
45. S.X. Dou, W.K. Yeoh, O. Shcherbakova, J. Horvat, J.H. Kim, A.V. Pan, D. Wexler, Y. Li, W.X. Li, Z.M. Ren, P. Munroe, J.Z. Cui, Appl. Phys. Lett. **89**(20), 202504–202506 (2006)
46. X.B. Zhu, H.C. Lei, S.B. Zhang, X.D. Zhu, B.S. Wang, G. Li, X. Luo, W.H. Song, J.M. Dai, Y.P. Sun, D.Q. Shi, S.X. Dou, Large magnetoresistance induced by surface ferromagnetism in A-type antiferromagnetic $La_{0.4}Sr_{0.6}MnO_3$ nanoparticles. J. Magn. Magn. Mater. **321**(13), 2009–2014 (2009)
47. J. Li, J. Wang, M. Wuttig, B. Ruette, D. Viehland, Dramatically enhanced polarization in (001), (101), and (111) $BiFeO_3$ thin films due to epitiaxial-induced transitions, Appl. Phys. Lett. **84**(1), 5261–5263 (2004)
48. R. Ramesh, N.A. Spaldin, Multiferroics: progress and prospects in thin films, Nature Mater. **6**(1), 21–29 (2007)
49. I. Sosnowska, T. Peterlin-Neumaier, E. Streichele, Spiral magnetic ordering in bismuth ferrite, J. Phys. C. **15**(23), 4835–4846 (1982)

50. Y.F. Popov, A.K. Zvezdin, G.P. Vorbev, V.A. Murashev, D.N. Racov, Linear magnetoelectric effect and phase transitions in bismuth ferrite, $BiFeO_3$, JETP Lett. **57**(1), 65–68 (1993)
51. F. Bai, J. Wang, P. Pyatakov, A.K. Zvezdin, L.E. Cross, Destruction of spin cycloid in **(111)c**-oriented **$BiFeO_3$** thin films by epitiaxial constraint: enhanced polarization and release of latent magnetization, Appl. Phys. Lett. **86**(1), 032511–032513 (2005)
52. C.F. Chung, J.P. Lin, J.M. Wu, Influence of Mn and Nb dopants on electric properties of chemical-solution-deposited $BiFeO_3$ film. Appl. Phys. Lett. **88**(24), 242909–242911 (2006)
53. G. Catalan, J.F. Scott, Physics and applications of bismuth ferrite. Adv. Mater. **21**(24), 2463–2485 (2009)
54. V.R. Singh, A. Garg, D.C. Agrawal, Structural changes in chemical solution deposited lanthanum doped bismuth ferrite thin films. Appl. Phys. Lett. **92**(1), 152905–152907 (2008)
55. F. Gao, C. Cai, Y. Wang, S. Dong, X.Y. Qiu, G.L. Yuan, Z.G. Liu, J.M. Liu, Preparation of La-doped $BiFeO_3$ thin films with Fe^{2+} ions on Si substrates. J. Appl. Phys. **99**(1), 094105–094110 (2006)
56. L.W. Martin, Y.H. Chu, M.B. Holcomb, M. Huijben, P. Yu, S.J. Han, D. Lee, S.X. Wang, R. Ramesh, Nanoscale control of exchange bias with $BiFeO_3$ thin films. NanoLett. **8**(7), 2050–2055 (2008)
57. Y.H. Chu, Q. He, C.H. Yang, P. Yu, L.W. Martin, P. Shafer, R. Ramesh, Nanoscale control of domain architectures in $BiFeO_3$ thin films. Nano Lett. **9**(4), 1726–1730 (2009)
58. S. Venkatesan, C. Daumont, B.J. Kooi, B. Noheda, J.T.M.D. Hosson, Nanoscale domain evolution in thin films of multiferroic $TbMnO_3$. Phys. Rev. B. **80**(1), 214111–214114 (2009)